Applied Mathematical Modelling 40 (2016) 5153–5170

Contents lists available at ScienceDirect

Applied Mathematical Modelling

journal homepage: www.elsevier.com/locate/apm

Comparison of two volume balance fully implicit approaches in conjunction with unstructured grids for compositional reservoir simulation

Bruno Ramon Batista Fernandes [a], Francisco Marcondes [b,*], Kamy Sepehrnoori [c]

[a] Laboratory of Computational Fluid Dynamics, Federal University of Ceará, Fortaleza, Brazil
[b] Department of Metallurgical Engineering and Materials Science, Federal University of Ceará, Fortaleza, Brazil
[c] Department of Petroleum and Geosystems Engineering, The University of Texas at Austin, Austin, USA

ARTICLE INFO

Article history:
Received 22 October 2014
Revised 9 June 2015
Accepted 9 September 2015
Available online 25 September 2015

Keywords:
Compositional simulation
EbFVM
IMPEC
Fully implicit
Unstructured grids

ABSTRACT

In reservoir simulation, compositional modeling is one of the most commonly used approaches for enhanced oil recovery processes. The methods used to solve the equations arising from the modeling of fluid flow in the reservoirs involve the degree of implicitness and the selection of the primary and secondary equations; primary and secondary variables have a great impact on the computational time. In this work, we implement and compare two fully implicit methods based on volume balance approach. The two methods share the same set of primary variables: pressure and total number of moles of each component. The total number of moles of each component is solved with use its material balance equation, whereas the pressure is solved with use of a volume balance equation. The difference between the two methods is in the nature of the volume balance equation. Whereas for one of the formulations the volume balance equation is the volume constraint and hence the only terms that appear in the Jacobian matrix are those from the volume in which the volume balance is evaluated, the second formulation considers an expanded form of the volume constraint. The main advantage of this expanded equation is that the Jacobian matrix involves information from the volume in which the balance is performed and from all neighboring volumes. The element-based finite-volume method in conjunction with unstructured grids for 2D and 3D reservoirs is used to discretize the material and volume balance equations. For two dimensions, quadrilateral and triangular elements are considered, whereas for three dimensions, hexahedral, prismatic, tetrahedral, and pyramidal elements are considered. The implementations were performed with the UTCOMP simulator developed at the University of Texas at Austin. We compare the performance of the two above-mentioned fully implicit formulations with the implicit pressure explicit composition (IMPEC) formulation of the UTCOMP simulator. The results of several case studies are compared in terms of volumetric oil and gas rates and the total CPU time. The results show good agreement between the production rates and saturation fields for all formulations. Additionally, the performance of the fully implicit methods was superior to that of the IMPEC method as a larger number of grid blocks were used in the simulations.

* Corresponding author. Tel.: +55 853366 9355; fax: +55 853366 9359.
E-mail address: marcondes@ufc.br (F. Marcondes).

http://dx.doi.org/10.1016/j.apm.2015.09.002
S0307-904X(15)00477-1/

1. Introduction

Petroleum reservoir simulation is an important tool used to forecast the oil and gas production rates as well as the amount of fluid that resides in the reservoir. In general, the modeling of the oil recovery processes consists of mass, volume, and energy balances that can reproduce the fluid dynamics inside the reservoir with the desired degree of realism and accuracy. These material balances form a nonlinear differential set of equations that cannot be solved without the use of numerical approaches unless several simplifications are made.

The reservoir simulation has evolved greatly since its introduction, not only in the physical modeling equations used but also in many other features, such as numerical formulations, gridding, flux approximation schemes, phase behavior calculations, geomechanics models, fractures and fault models, and linear solvers. Fussel and Fussel [1] were the first authors to develop a simulator using an equation of state for both phase equilibrium and density calculations. They used the constraint equations (equilibrium equations and volume constraint) to solve n_c+1 primary variables and the flow equations to solve the secondary variables. Coats [2] presented the first fully implicit (FI) formulation for the isothermal compositional model. He used a Gaussian elimination to decouple the primary variables from the secondary variables. Nghiem et al. [3] developed an implicit pressure explicit saturation (IMPES) formulation that differs from the previously mentioned formulations by solving pressure and compositions separately. Young and Stephenson [4] developed a new approach based on the formulation proposed in [1] which is also an implicit pressure explicit composition (IMPEC) approach. The major difference between these two approaches resides in the selection of the primary variables and in the ordering of the equations. Another FI model was proposed by Chien et al. [5]. In this model, the primary equations are obtained from the material balance equations of each component. They proposed a set of primary variables similar to that proposed by Coats [2], except that gas mole fractions were replaced by the equilibrium ratios (K values). Ács et al. [6] proposed a new IMPES formulation that shares the primary variables of Kazemi et al. [7] and Nghiem et al. [3]. Although the pressure equation is based on a volume balance as in the other two models, it is obtained in a special way that allows the formulation to perform just one flash calculation per time step. Watts [8] combined the one iteration per time step idea of Ács et al. [6] with the sequential implicit pressure and saturations (IMPSAT) formulation of Spillette et al. [9] to generate a new IMPSAT formulation. Quandalle and Savary [10] extended the formulation of Watts to solve an inconsistency of this formulation. They included the solution of n_c-2 new variables in the material balance equations. The new variables can be solved in terms of oil or gas compositions. Collins et al. [11] presented an adaptive implicit approach for an isothermal compositional formulation. The equations for this formulation are the n_c+1 material balances and the volume constraint. The primary variables are the total number of moles per bulk volume of the n_c components and water. Branco and Rodriguez [12] proposed a new IMPSAT formulation based on the formulation of Coats [2]. Wang et al. [13] proposed a new FI formulation. In this formulation the flow equations and the equilibrium constraints are all assembled into the Jacobian matrix. Haukas et al. [14] improved the approach of Quandalle and Savary [10] by changing the primary variables. Haukas et al. [15] gave a better interpretation of these parameters. They called the new parameters "isochoric parameters." A stability criterion was also given in [15]. Santos et al. [16, 17] implemented and compared the following approaches: the FI formulations of Coats [2], Collins et al. [11], and Wang et al. [13], the IMPSAT formulation of Branco [12], and an IMPES formulation. Fernandes et al. [18] compared the formulation of Ács et al. [6] with the formulation of Watts [8].

Most of the formulations presented previously used Cartesian grids in conjunction with the finite-volume method (FVM). However, all the formulations can be implemented for any spatial discretization since their derivations are independent of the grid discretization. However, as the Cartesian grid is the simplest way to discretize the domain, the complexity of the implementation of a given formulation for other types of grids will increase sharply. The unstructured grids are more general in terms of modeling important features of the reservoirs. The unstructured grids are usually related to the concept of elements. However, for many years this concept was used only in the finite-element method (FEM) until the pioneer work of Baliga and Patankar [19] that combined the conservative approach of the FVM with the idea of elements and shape functions of the FEM, creating a new method that they named the "control volume finite-element method" (CVFEM). Later, Maliska [20] suggested that the CVFEM denomination is unsuitable, since the CVFEM gives the wrong idea that we have a finite-element approach that is based on material balance. Maliska [20] suggested that "element-based finite-volume method" (EbFVM) is a more appropriate denomination since we still have an approach that locally respects the material balance of the physical property being transported. For this reason, in the rest of this article, we will always refer to this approach as the EbFVM.

The first use of unstructured grids in reservoir simulation was by Heinemann and Brand [21] and Heinemann et al. [22] in conjunction with perpendicular bisector (PEBI) grids. These grids are also called "Voronoi grids." Like the Cartesian grids, the PEBI are cell-center grids and therefore are used for isotropic media, and it is possible to evaluate fluxes with use of only two grid points. The first use of the EbFVM in reservoir simulation was by Rozon [23]; he used it to solve a single-phase flow using quadrilateral elements. Rozon [23] also presented a comparison of the truncation errors between the EbFVM and the Cartesian grids, showing that for regular grids composed of quadrilateral elements the EbFVM is more accurate. Fung et al. [24] used PEBI grids based on triangular elements in a thermal general-purpose simulator. Cordazzo [25] solved the two-phase flow (water and oil) in conjunction with the EbFVM using triangular and quadrilateral elements. Marcondes and Sepehrnoori [26] used the EbFVM for the FI isothermal compositional simulation in conjunction with triangular and quadrilateral elements. Recently, Marcondes et al. [27] and Santos et al. [28] implemented the EbFVM for 3D isothermal compositional reservoir simulation using four element types: hexahedron, tetrahedron, pyramid, and prism. Also, using the EbFVM approach, Fernandes et al. [29] has investigated the use of several interpolation functions in conjunction with 2D compositional reservoir simulation. More recently, Fernandes et al.

[30] adapted the total variation diminishing scheme for the cell-center approach of Darwish and Moukaled [31] to the 3D EbFVM in conjunction with hexahedral elements using the MINMOD [32] and Koren [33] flux limiters.

In this work, the FI formulation of Collins et al. [11] and an FI version of the formulation of Ács et al. [6] are implemented in the UTCOMP simulator. The UTCOMP simulator is a multicomponent/multiphase simulator that takes into account up to four phases that was developed at the University of Texas at Austin. The two FI approaches implemented in this work are compared with the original IMPEC formulation of Ács et al. [6] originally implemented in the UTCOMP simulator with use of Cartesian grids [34] and the EbFVM [35,36,37]. These implementations can be further improved by parallel processing using, for instance, a message passing interface as was done by Doroh [38], who extended the UTCOMP simulator's IMPEC serial formulation into a parallel framework, and by Wang et al. [39], who implemented and tested a framework to run the GPAS simulator in parallel was developed, an FI reservoir simulator. Efforts are currently being devoted to the parallelization of the UTCOMP simulator in conjunction with unstructured grids.

2. Physical model

The flow equations of all formulations implemented here consist of material balance equations and one volume balance equation. Additionally, all formulations considered here share the same set of primary variables: oil pressure and total number of moles of each component.

The volume balance equation used to compute pressure for the formulation of Ács et al. [6] is as follows:

$$\left(\phi^0 C_f - \frac{1}{V_b}\frac{\partial V_T}{\partial P}\right)\frac{\partial P}{\partial t} = \bar{V}_{Tw}\vec{\nabla}\cdot\left(\xi_w \frac{k_{rw}}{\mu_w}\bar{\bar{K}}\cdot\vec{\nabla}\Phi_w\right) + \sum_{k=1}^{n_c}\bar{V}_{Tk}\sum_{j=2}^{n_p}\vec{\nabla}\cdot\left(x_{kj}\xi_j\frac{k_{rj}}{\mu_j}\bar{\bar{K}}\cdot\vec{\nabla}\Phi_j\right) - \sum_{k=1}^{n_c+1}\bar{V}_{Tk}\frac{\dot{q}_k}{V_b}, \tag{1}$$

where P is the oil pressure, V_T is the total fluid volume, C_f is the formation compressibility, and k_{rj}, ξ_j,, and μ_j are the relative permeability, the molar density, and the viscosity of the jth phase, respectively. $\bar{\bar{K}}$ is the absolute permeability tensor, .. is the partial derivative of the total fluid volume with respect to the total number of moles of component k, V_b is the bulk volume, x_{kj} is the molar fraction of component k in phase j, ϕ is the porosity, $\dot{q}_k$ is the source/sink term of component k due to the producing/injecting well, and Φ_j is the hydraulic potential of phase j defined as follows:

$$\Phi_j = P + P_{cjo} - \rho_j g D j = 1,\ldots,n_p, \tag{2}$$

where P_{cjo} is the capillary pressure of phase j related to the oil phase, g is the gravitational acceleration, D is the depth, which is positive in a downward direction, and ρ_j is the mass density of phase j.

The volume balance equation used to compute pressure for the formulation of Collins et al. [11] is as follows:

$$\phi = \frac{1}{V_b}\sum_{j=1}^{n_p}\frac{n_j}{\xi_j}, \tag{3}$$

where n_j is the number of moles of phase j.

The formulations of Ács et al. [6] and Collins et al. [11] share the same material balance equations for determination of the total number of moles of each component. The hydrocarbon and water mole balance equations are as follows:

$$\frac{1}{V_b}\frac{\partial N_k}{\partial t} = \sum_{j=2}^{n_p}\vec{\nabla}\cdot\left(x_{kj}\xi_j\frac{k_{rj}}{\mu_j}\bar{\bar{K}}\cdot\vec{\nabla}\Phi_j\right) - \frac{\dot{q}_k}{V_b}, \quad k = 1,\ldots,n_c \tag{4}$$

and

$$\frac{1}{V_b}\frac{\partial N_w}{\partial t} = \vec{\nabla}\cdot\left(\xi_w\frac{k_{rw}}{\mu_w}\bar{\bar{K}}\cdot\vec{\nabla}\Phi_w\right) - \frac{\dot{q}_w}{V_b}, \tag{5}$$

respectively, where N_k is the total number of moles of component k.

The Peng–Robinson equation of state [40] is used to compute density and fugacities.

The phase appearance and disappearance is treated by means of a stability test calculation. Two phase stability test algorithms are implemented in the UTCOMP simulator: the stationary point location method [41] and the Gibbs free energy minimization algorithm, which is similar to the method of Trangenstein [42] and was modified by Perschke [43] to deal with the equilibrium of three hydrocarbon phases. In general, as mentioned by Perschke [43], the stationary method is faster than the Gibbs free energy minimization method.

After the phase stability calculation to evaluate the mole fractions and amount of each hydrocarbon phase is performed. The flash calculation used in the UTCOMP simulator is a combination of the accelerated successive substitution method [44] and the modified version of the Gibbs free energy minimization method [43]. At the beginning of the flash procedure, we use the accelerated successive substitution method to provide a reasonable initial estimation, and then we switch to the Gibbs free energy minimization method to accelerate the convergence. The switching criterion to change from one method to another is given by [34] following:

$$\max\left|\ln f_{ij} - \ln f_{ir}\right| \le \varepsilon_{swi}, \quad i = 1,\ldots,n_c, \quad j = 2,\ldots,n_p(j \ne r), \tag{6}$$

where r is a reference phase, generally assumed to be the oil phase. The switching criterion (ε_{swi}) suggested in [34] is equal to 0.01.

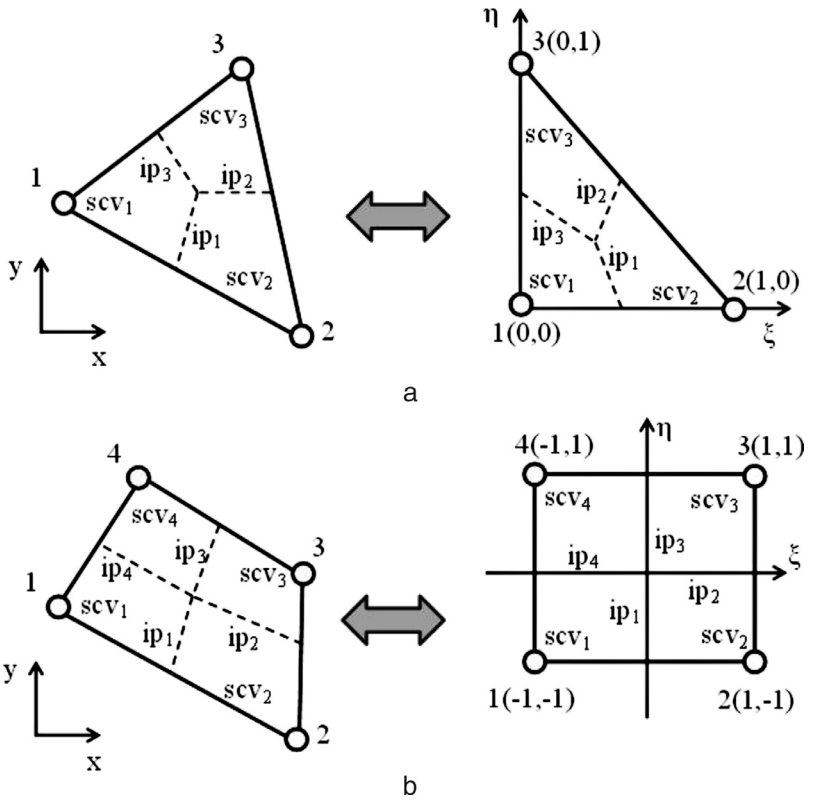

Fig. 1. Two-dimensional elements in the physical and computational planes: (a) triangular element; (b) quadrilateral element.

3. Approximate equations

In the EbFVM the domain is divided into elements. The elements used to discretize 2D reservoirs are triangular and quadrilateral, and hexahedral, tetrahedra, prismatic, and pyramidal elements are used to discretize 3D reservoirs, as shown in Figs. 1 and 2, respectively.

The physical properties are easily approximated inside each element with use of shape functions. The shape functions for each element are not shown in this work but can be found in the literature [20,27,45].

The gradient inside any element is evaluated with use of the shape functions as follows:

$$\frac{\partial \phi}{\partial x} = \sum_{i=1}^{n_v} \frac{\partial N_i}{\partial x}\Phi_i;\ \frac{\partial \phi}{\partial y} = \sum_{i=1}^{n_v} \frac{\partial N_i}{\partial y}\Phi_i;\ \frac{\partial \phi}{\partial z} = \sum_{i=1}^{n_v} \frac{\partial N_i}{\partial z}\Phi_i, \tag{7}$$

where N is the shape function and Φ is an arbitrary property evaluated at the vertex of the element.

The derivatives of the shape functions with respect to x, y, and z are obtained for 3D elements as follows:

$$\begin{aligned}
\frac{\partial N_i}{\partial x} &= \frac{1}{\det(J_t)}\left[\left(\frac{\partial y}{\partial \eta}\frac{\partial z}{\partial \gamma} - \frac{\partial y}{\partial \gamma}\frac{\partial z}{\partial \eta}\right)\frac{\partial N_i}{\partial \xi} - \left(\frac{\partial y}{\partial \xi}\frac{\partial z}{\partial \gamma} - \frac{\partial y}{\partial \gamma}\frac{\partial z}{\partial \xi}\right)\frac{\partial N_i}{\partial \eta} + \left(\frac{\partial y}{\partial \xi}\frac{\partial z}{\partial \eta} - \frac{\partial y}{\partial \eta}\frac{\partial z}{\partial \xi}\right)\frac{\partial N_i}{\partial \gamma}\right];\\
\frac{\partial N_i}{\partial y} &= \frac{1}{\det(J_t)}\left[\left(\frac{\partial x}{\partial \eta}\frac{\partial z}{\partial \gamma} - \frac{\partial x}{\partial \gamma}\frac{\partial z}{\partial \eta}\right)\frac{\partial N_i}{\partial \xi} + \left(\frac{\partial x}{\partial \xi}\frac{\partial z}{\partial \gamma} - \frac{\partial x}{\partial \gamma}\frac{\partial z}{\partial \xi}\right)\frac{\partial N_i}{\partial \eta} - \left(\frac{\partial x}{\partial \xi}\frac{\partial z}{\partial \eta} - \frac{\partial x}{\partial \eta}\frac{\partial z}{\partial \xi}\right)\frac{\partial N_i}{\partial \gamma}\right];\\
\frac{\partial N_i}{\partial z} &= \frac{1}{\det(J_t)}\left[\left(\frac{\partial x}{\partial \eta}\frac{\partial y}{\partial \gamma} - \frac{\partial x}{\partial \gamma}\frac{\partial y}{\partial \eta}\right)\frac{\partial N_i}{\partial \xi} - \left(\frac{\partial x}{\partial \xi}\frac{\partial z}{\partial \gamma} - \frac{\partial x}{\partial \gamma}\frac{\partial y}{\partial \xi}\right)\frac{\partial N_i}{\partial \eta} + \left(\frac{\partial x}{\partial \xi}\frac{\partial y}{\partial \eta} - \frac{\partial x}{\partial \eta}\frac{\partial y}{\partial \xi}\right)\frac{\partial N_i}{\partial \gamma}\right],
\end{aligned} \tag{8}$$

where,

$$\det(J_t) = \frac{\partial x}{\partial \xi}\left(\frac{\partial y}{\partial \eta}\frac{\partial z}{\partial \gamma} - \frac{\partial y}{\partial \gamma}\frac{\partial z}{\partial \eta}\right) - \frac{\partial x}{\partial \eta}\left(\frac{\partial y}{\partial \xi}\frac{\partial z}{\partial \gamma} - \frac{\partial y}{\partial \gamma}\frac{\partial z}{\partial \xi}\right) + \frac{\partial x}{\partial \gamma}\left(\frac{\partial y}{\partial \xi}\frac{\partial z}{\partial \eta} - \frac{\partial y}{\partial \eta}\frac{\partial z}{\partial \xi}\right). \tag{9}$$

For 2D elements, a similar expression is obtained:

$$\frac{\partial N_i}{\partial x} = \frac{1}{\det(J_t)}\left(\frac{\partial y}{\partial \eta}\frac{\partial N_i}{\partial \xi} - \frac{\partial y}{\partial \xi}\frac{\partial N_i}{\partial \eta}\right);\ \frac{\partial N_i}{\partial y} = \frac{1}{\det(J_t)}\left(\frac{\partial x}{\partial \xi}\frac{\partial N_i}{\partial \eta} - \frac{\partial x}{\partial \eta}\frac{\partial N_i}{\partial \xi}\right), \tag{10}$$

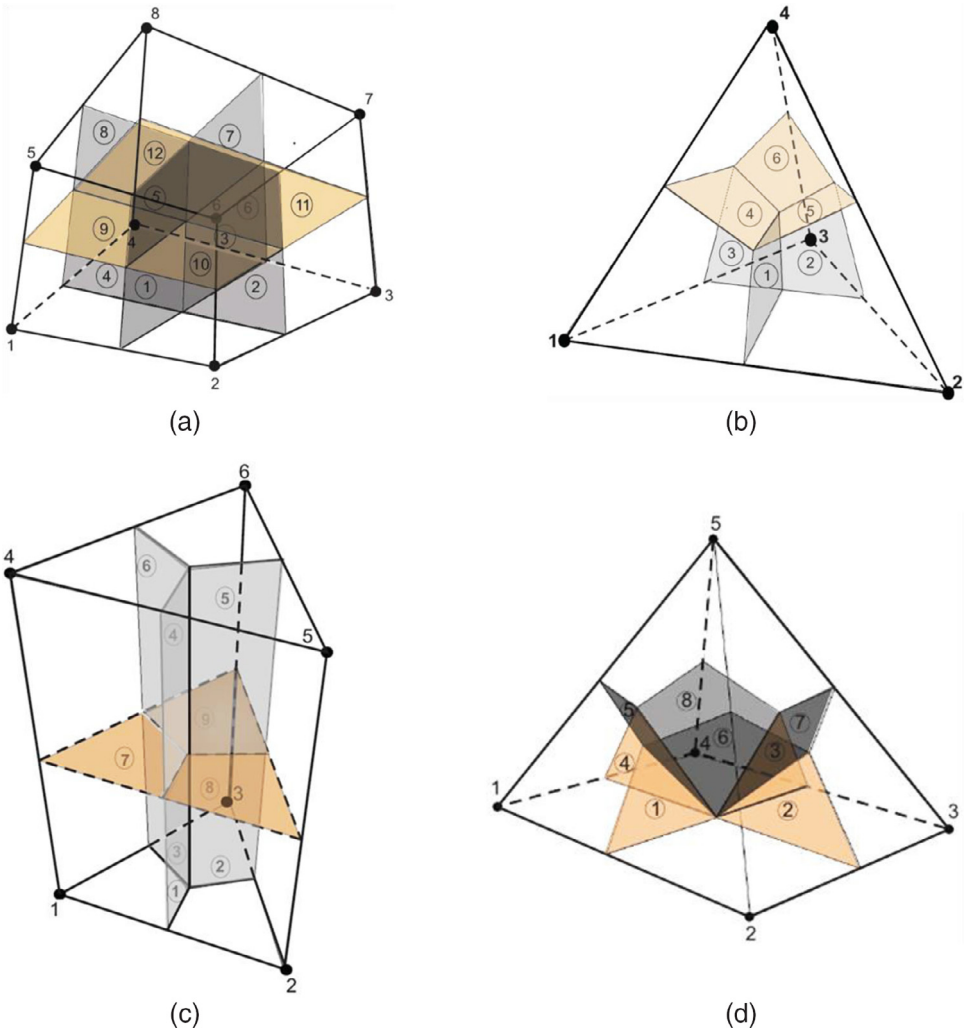

Fig. 2. Three-dimensional elements: (a) hexahedral element; (b) tetrahedral element; (c) prismatic element; (d) pyramidal element.

where,

$$\det(J_t) = \left(\frac{\partial x}{\partial \xi}\frac{\partial y}{\partial \eta} - \frac{\partial x}{\partial \eta}\frac{\partial y}{\partial \xi}\right). \tag{11}$$

The interface areas for 3D elements are computed as follows:

$$d\vec{A} = \left(\frac{\partial y}{\partial m}\frac{\partial z}{\partial n} - \frac{\partial y}{\partial n}\frac{\partial z}{\partial m}\right)dmdn\hat{i} - \left(\frac{\partial x}{\partial n}\frac{\partial z}{\partial m} - \frac{\partial x}{\partial m}\frac{\partial z}{\partial n}\right)dmdn\hat{j} + \left(\frac{\partial x}{\partial m}\frac{\partial y}{\partial n} - \frac{\partial x}{\partial n}\frac{\partial y}{\partial m}\right)dmdn\hat{k}, \tag{12}$$

where m and n are any of the coordinates ξ, η, or γ. For 2D elements, the area of each interface, reading counterclockwise, is given by following:

$$d\vec{A} = h\left(dy\hat{i} - dx\hat{j}\right), \tag{13}$$

where h is the thickness of the reservoir. Further details on the above expressions can be found in [20,26].

Each element is divided into subelements according to the number of vertices. Next, the conservative equations are integrated for each of these subelements. These subelements are called "sub–control volumes" (SCVs). After the conservative equations have been integrated for each of these SCVs, we assemble the control volume equations by obtaining the contributions of all SCVs that share the same vertex of the grid. This feature is called "dual mesh" and gives rise to a cell-vertex approach. The great advantage of this approach is that all calculations are based on only the elements of the grid. The dual mesh is illustrated in Fig. 3. As presented in Fig. 3, the blue labels represent the elements and the black labels represent the control volumes. The control volume associated with vertex 5 of the grid shown in Fig. 3 is given by the green area.

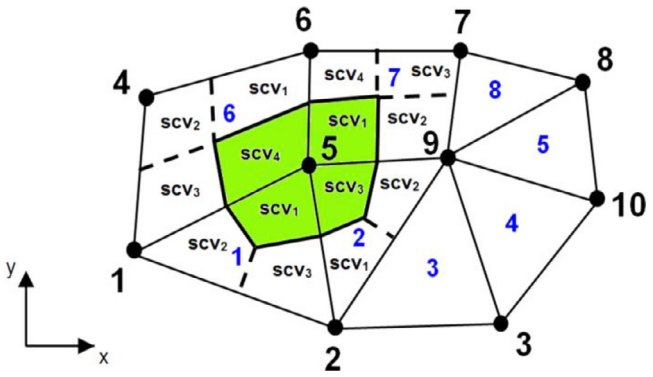

Fig. 3. A dual mesh for the EbFVM approach. (For interpretation of the references to colour in this figure legend, the reader is referred to the web version of this article.)

As previously mentioned, for the EbFVM each term of the conservation equation is integrated for each SCV. Then, the contribution of each SCV is summed to obtain the closure of each control volume associated with each vertex of the grid. These calculations are computed at an element level. For the mole balance equations, for instance, the integration in space and time, for the SCVs of each element of the grid, can be written as follows:

$$A_{cc_i}^{N_k} - F_{adv_i}^{N_k} - S_i^{N_k} = 0, \quad k = 1, \ldots, n_c + 1; \quad i = 1, \ldots, n_v, \tag{14}$$

where n_v is the number of vertices of the element, $A_{cc_i}^{N_k}$ denotes the accumulation term of component k in SCV i, $F_{adv_i}^{N_k}$ denotes the advective net flux of component k across the SCV i interfaces, and $S_i^{N_k}$ denotes the source/sink (wells) term of component k in SCV i. These terms for the hydrocarbon components and water are given below:

$$A_{cc_i}^{N_k} = \left(\frac{N_{k,i}^{n+1} - N_{k,i}^{n}}{V_{b,i}}\right) V_{scv_i}, \quad k = 1, \ldots, n_c + 1; \quad i = 1, \ldots, n_v, \tag{15}$$

$$F_{adv_i}^{N_k} = \Delta t \sum_{j=2}^{n_p} \sum_{l=1}^{n_{ip}} \left[\left(x_{kj}^{n+1} \xi_j^{n+1} \frac{k_{rj}^{n+1}}{\mu_j^{n+1}} \sum_{m=1}^{n_v} \Upsilon_{iml} \left(P_m^{n+1} + P_{cjr,m}^{n+1} - \rho_{j,elem}^{n+1} g D_m \right) \right) \right]_l,$$
$$k = 1, \ldots, n_c; i = 1, \ldots, n_v. \tag{16}$$

$$F_{adv_i}^{N_{n_c+1}} = \Delta t \sum_{l=1}^{n_{ip}} \left[\left(\xi_j^{n+1} \frac{k_{rj}^{n+1}}{\mu_j^{n+1}} \sum_{m=1}^{n_v} \Upsilon_{iml} \left(P_m^{n+1} + P_{cjr,m}^{n+1} - \rho_{j,elem}^{n+1} g D_m \right) \right) \right]_l,$$
$$i = 1, \ldots, n_v. \tag{17}$$

and

$$S_i^{N_k} = -\Delta t \frac{V_{SCV_i}}{V_{b,i}} q_{k,i}^{n+1}, k = 1, \ldots, n_c + 1; i = 1, \ldots, n_v, \tag{18}$$

where n_c+1 denotes the water component, V_{SCV_i} is the volume of SCV i, and n_{ip} is the number of integration points of SCV i. For 2D elements (triangles and quadrilaterals), the number of integration points is always two. For 3D elements, the number of integration points of a given SCV is usually three, except for the SCV associated with the apex of the pyramid, which has four integration points; see Fig. 2d. The Υ term in Eqs. (16) and (17) involves only geometric and absolute permeability tensors and is defined by following:

$$\Upsilon_{iml} = \bar{\bar{K}}_l \cdot \vec{\nabla} N_{m,l} \cdot \Delta \vec{A}_l, \tag{19}$$

where Υ_{iml} is the Υ term associated with SCV i and is evaluated at integration point l.

For the formulation of Ács et al. [6], the accumulation, advection, and well terms for the pressure equation are written as follows:

$$A_{cc_i}^{P} = \left[V_{scv_i} \phi_{elem}^{0} C_f - \frac{V_{scv_i}}{V_{b,i}} \frac{\partial V_{T,i}^{n}}{\partial P} \right] \left(P_i^{n+1} - P_i^{n} \right) - \frac{V_{scv_i}}{V_{b,i}} \left(V_{T,i}^{n} - V_{p,i}^{n} \right), \quad i = 1, \ldots, n_v, \tag{20}$$

$$F^P_{adv_i} = \Delta t \bar{V}^n_{Tw,i} \sum_{l=1}^{n_{ip}} \left[\left(\xi^{n+1}_w \frac{k^{n+1}_{rw}}{\mu^{n+1}_w} \sum_{m=1}^{n_v} \Upsilon_{iml} \left(P^{n+1}_m + P^{n+1}_{cwr,m} - \rho^{n+1}_{w,elem} g D_m \right) \right) \right]_l + \Delta t \sum_{k=1}^{n_c} \bar{V}^n_{Tk,i} \sum_{j=2}^{n_p} \sum_{l=1}^{n_{ip}} \left[\left(x^{n+1}_{kj} \xi^{n+1}_j \frac{k^{n+1}_{rj}}{\mu^{n+1}_j} \sum_{m=1}^{n_v} \Upsilon_{iml} \left(P^{n+1}_m + P^{n+1}_{cjr,m} - \rho^{n+1}_{j,elem} g D_m \right) \right) \right]_l, \quad i = 1, \ldots, n_v, \tag{21}$$

$$S^P_i = \Delta t \sum_{k=1}^{n_c+1} \bar{V}^n_{Tk,i} \frac{V_{SCV_i}}{V_{b,i}} \dot{q}^{n+1}_{k,i}, \quad i = 1, \ldots, n_v, \tag{22}$$

respectively.

For the formulation of Collins et al. [11], the terms for the pressure equation are given by

$$A^P_{cc_i} = V_{scv_i} \phi^{n+1}_i - \frac{V_{scv_i}}{V_{b,i}} \sum_{j=1}^{n_p} \frac{n^{n+1}_{j,i}}{\xi^{n+1}_{j,i}}, \quad i = 1, \ldots, n_v, \tag{23}$$

$$F^P_{adv_i} = 0, \quad i = 1, \ldots, n_v, \tag{24}$$

$$S^P_i = 0, \quad i = 1, \ldots, n_v. \tag{25}$$

From Eqs. (23)–(25), we can see that there is no coupling between the control volume and its neighbors, as we have for the pressure equation in the formulation of Ács et al. [6]. For simplicity, we will refer to the FI formulation of Collins et al. [11] as FI-0, and we will refer to the FI formulation proposed in this work derived from the formulation of Ács et al. [6] as FI-1.

The discretized equations for both FI-0 and FI-1 are strongly nonlinear in the primary variables. Hence, an exact Newton method is used to solve the set of nonlinear equations for both FI approaches. The linear system of equations that arises for each Newton linearization is solved with use of the default options in the PETSC library [46], which uses GMRES [47] preconditioned on the left with an ILU(0) as the default solver.

4. Results and discussion

Three case studies for testing and verification of the FI formulations implemented in this work in conjunction with Cartesian and unstructured grids are presented. The results will be compared in terms of oil and gas production rates, time-step profiles, phase saturation fields, and overall CPU time. We validate all the new formulations with the original IMPEC formulation of the UTCOMP simulator, since it was severely tested and compared with several commercial simulators [48]. The field profiles are visualized with the ESSS Kraken® postprocessor.

In contrast to the IMPEC formulation, FI formulations can theoretically use large time steps. However, the use of large time steps can lead to loss of accuracy. Therefore, a time refinement needs to be performed to ensure that a time-independent solution is obtained. For this reason, all results presented in this section were obtained after a time refinement had been performed. Furthermore, all runs used a time-step control based on variations in pressure, saturations, and rate of change in the number of moles of each component as described in [34]. The time-step size is also allowed to vary within a range of minimum and maximum time steps. For most of the simulations, both FI formulations used the maximum time step for most periods of the simulations.

All fluid properties used in the equation of state and the relative permeability parameters of the modified Stone II model [49] are shown in the tables in Appendix A. Capillary pressure is not considered in any of the case studies, but it was implemented and tested for both FI formulations.

Case study 1 consists of production, in a quarter-of-a five-spot configuration, of a heavy oil characterized by three components: CO_2, C_1, and nC_{16}. The reservoir initially contains only water and oil phases. A fluid rich in CO_2 is injected, which creates a new phase in the reservoir. Only immobile water exists in the reservoir during the whole simulation. Table 1 presents the reservoir data used for this case. The equation of state parameters used for this case study is shown in Tables A1 and A3, and the relative permeability parameters are presented in Table A5.

Two-dimensional and three-dimensional reservoirs with unstructured grids are considered for this case study. When one is using unstructured grids, it is important to see if the grid distortion has any impact on the performance of the formulations. Therefore, for this case study, the formulations are first run for regular grids of quadrilateral elements, and are then run for nonuniform grids of quadrilateral and triangular elements. Fig. 4 presents the finest grids used for each of these element types.

The oil and gas production rates obtained with the FI approaches and the IMPEC formulation for the grid shown in Fig. 4a are presented in Fig. 5. From this figure, one can see there is good agreement between the production rate curves. The production rates for the other grids are not displayed because they are very similar to the ones presented in Fig. 5.

The gas saturation field at 500 days obtained with all the grids presented in Fig. 4 is presented in Fig. 6. From this figure, one can see there is good agreement between the saturation fields obtained with all formulations.

Table 1
Reservoir data for cases 1 and 2.

Property	Value
Length, width, and thickness	243.83 m, 243.83 m, and 60.96 m
Porosity	0.30
Initial water saturation	0.25
Initial pressure	20.65 MPa
Permeability in x, y, and z directions	1.97×10^{-13} m^2, 1.97×10^{-13} m^2, and 1.97×10^{-14} m^2
Formation temperature	299.82 K
Gas injection rate	5.66×10^{5} m^3/day
Producer's bottom hole pressure	20.65 MPa
Reservoir's initial composition (CO_2, C_1, and nC_{16})	0.01, 0.19, and 0.80
Injection fluid composition (CO_2, C_1, and nC_{16})	0.95, 0.05 and 0.00

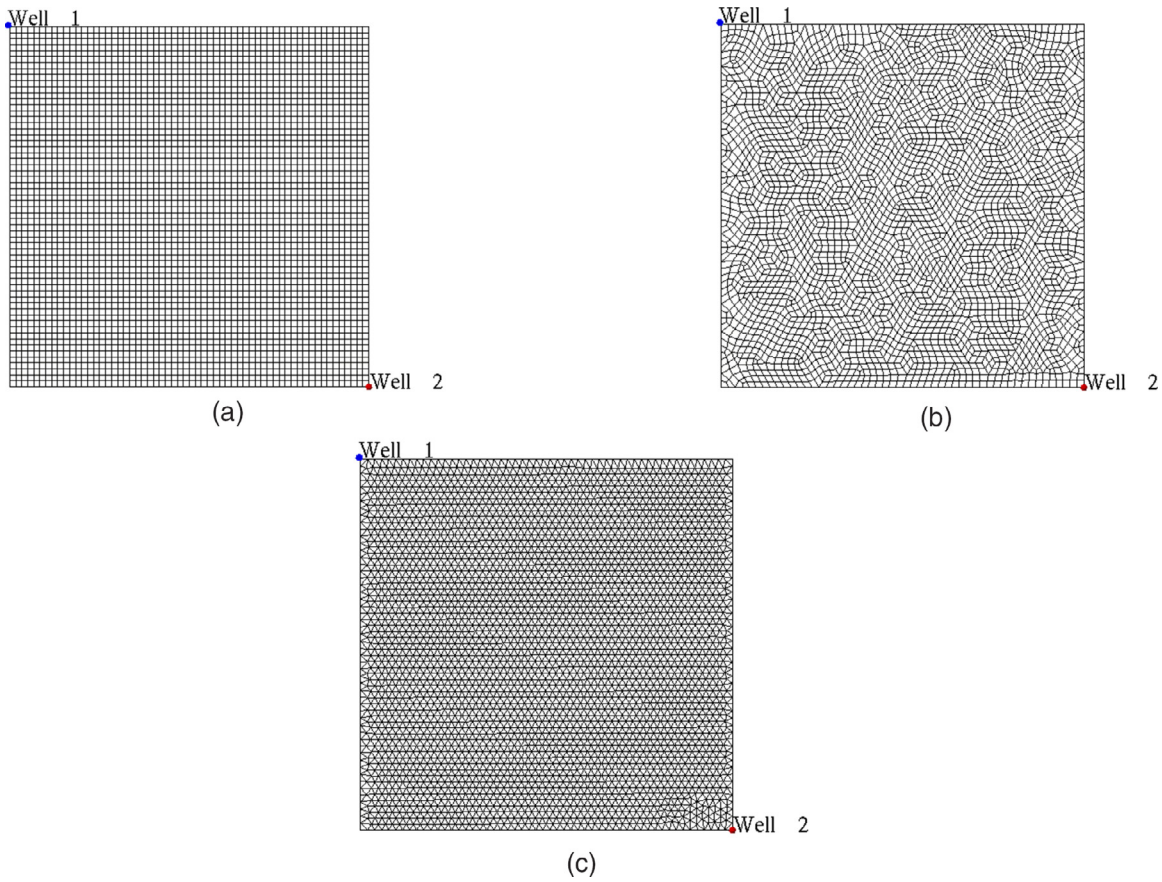

Fig. 4. Finest grids—case 1: (a) 60 × 60 grid; (b) quadrilateral unstructured grid with 3387 vertices (3282 elements); (c) triangular unstructured grid with 3329 vertices (6444 elements).

The CPU times for all formulations, the total number of Newton iterations, and the total number of time steps for the FI approaches using regular quadrilateral grids are presented in Table 2. The same information is presented for the unstructured quadrilateral and triangular grids in Tables 3 and 4, respectively. As one can observe, for coarse grids, the performances of the FI approaches are worse than the performance for the IMPEC formulation owing to the small Courant-Friedrichs-Lewy number. When the grids are refined, the FI approaches outperform the IMPEC approach in terms of CPU time. Additionally, in general, FI-1 was faster than FI-0 for this case. From the tables, it can also be seen that the FI-1 approach requires slightly more Newton iterations than the FI-0 approach, but requires less CPU time because it seems that the linear system of the FI-1 approach is better conditioned owing to the tighter coupling between the equations.

In case 2, the same fluid and reservoir configuration used in case 1 is used. The main difference here is that now the reservoir domain is discretized with use of 3D elements and gravity is now considered. In this analysis, four sets of 3D unstructured grids composed only of hexahedrons, tetrahedrons, prisms, and pyramids, respectively, were used. The finest grid of each set is presented in Fig. 7.

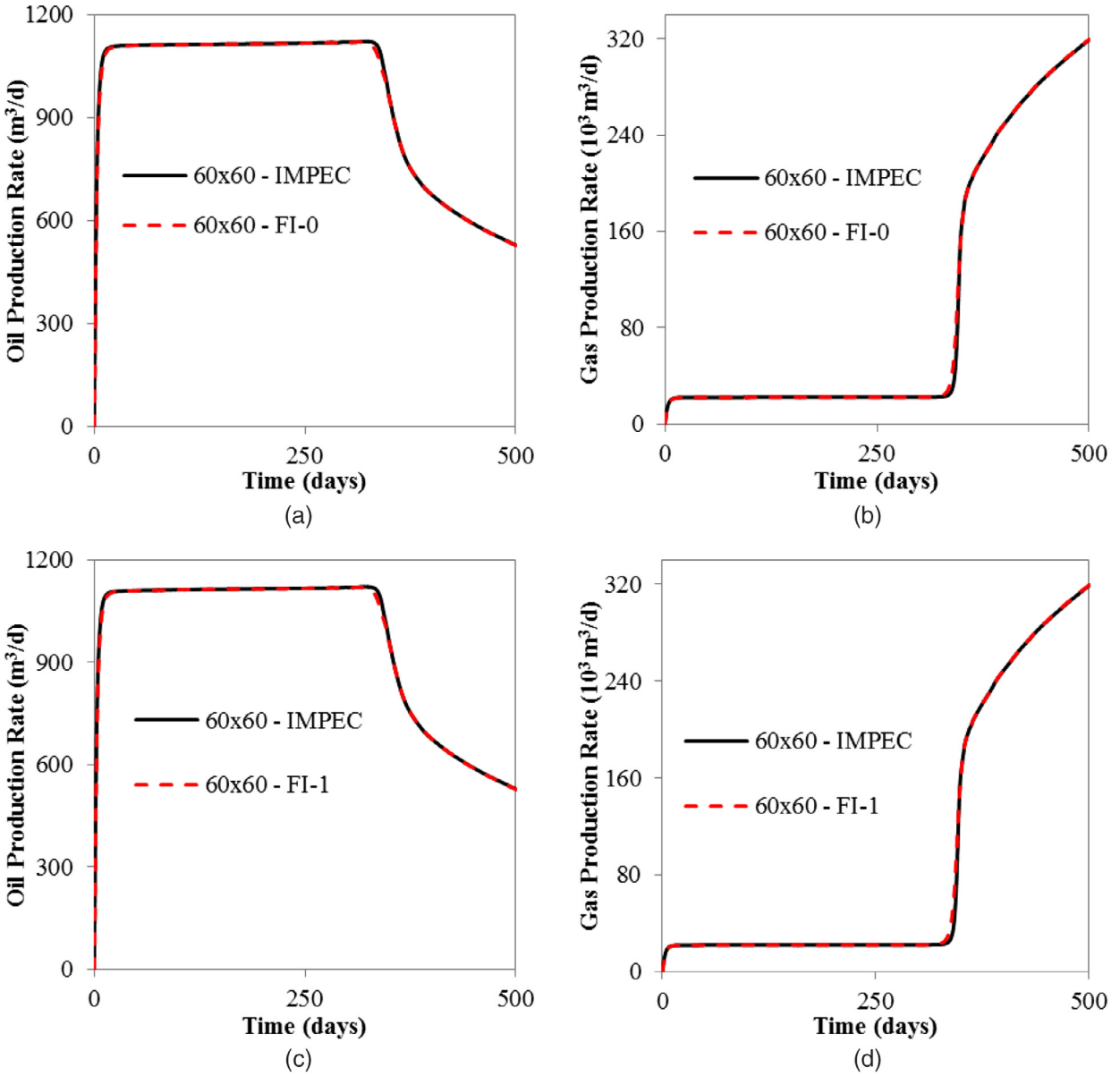

Fig. 5. Production rates—case 1 using 2D regular quadrilateral grids: (a) IMPEC versus FI-0, oil; (b) IMPEC versus FI-0, gas; (c) IMPEC versus FI-1, oil; (d) IMPEC versus FI-1, gas.

Table 2
CPU times, number of Newton iterations, and number of time steps. Two-dimensional regular quadrilateral grids—case 1.

Result	20 × 20	40 × 40	60 × 60
IMPEC CPU time (s)	15.2	272.6	1540.7
FI-0 CPU time (s)	18.6	179.3	797.4
FI-1 CPU time (s)	18.7	184.6	732.5
Number of Newton iterations for FI-0	1124	1286	1429
Number of Newton iterations for FI-1	1133	1297	1434
Number of time steps for FI-0	540	523	525
Number of time steps for FI-1	540	523	525

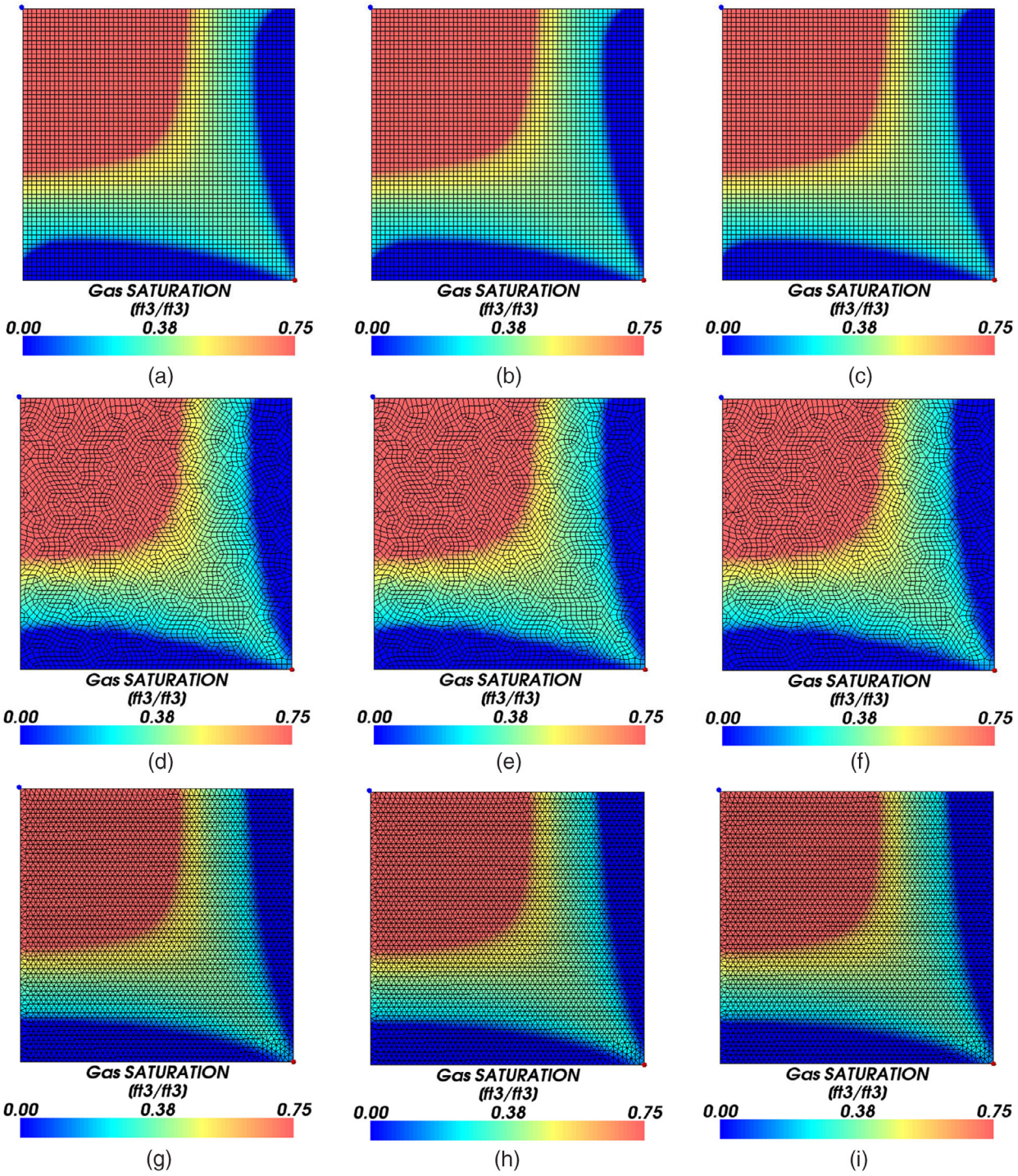

Fig. 6. Gas saturation field at 500 days—case 1: (a) quadrilateral, 60 × 60, IMPEC; (b) quadrilateral, 60 × 60, FI-0; (c) quadrilateral, 60 × 60, FI-1; (d) quadrilateral, 3387 vertices, IMPEC; (e) quadrilateral, 3387 vertices, FI-0; (f) quadrilateral, 3387 vertices, FI-1; (g) triangular, 3329 vertices, IMPEC; (h) triangular, 3329 vertices, FI-0; (i) triangular, 3329 vertices, FI-1.

Table 3
CPU times, number of Newton iterations, and number of time steps. Two-dimensional unstructured quadrilateral grids—case 1.

Result	1199 vertices	2661 vertices	3387 vertices
IMPEC CPU time (s)	113.8	699.2	954.6
FI-0 CPU time (s)	110	470.3	463.3
FI-1 CPU time (s)	108.6	402.5	420.1
Number of Newton iterations for FI-0	1271	1421	1448
Number of Newton iterations for FI-1	1272	1425	1449
Number of time steps for FI-0	512	522	514
Number of time steps for FI-1	512	522	514

Table 4
CPU times, number of Newton iterations, and number of time steps. Two-dimensional unstructured triangular grids—case 1.

Result	1220 vertices	2330 vertices	3329 vertices
IMPEC CPU time (s)	109.6	649.2	1354.4
FI-0 CPU time (s)	89.1	301.2	582.8
FI-1 CPU time (s)	85.9	269.6	566
Number of Newton iterations for FI-0	1277	1390	1446
Number of Newton iterations for FI-1	1281	1397	1446
Number of time steps for FI-0	520	525	525
Number of time steps for FI-1	520	525	525

Table 5
CPU times, number of Newton iterations, and number of time steps. Three-dimensional hexahedral grids—case 2.

Result	1024 vertices	6480 vertices	11,767 vertices
IMPEC CPU time (s)	36.1	1325.7	3590.8
FI-0 CPU time (s)	170.4	1525.5	3191.2
FI-1 CPU time (s)	179.9	1335.7	3188.6
Number of Newton iterations for FI-0	1086	1535	1565
Number of Newton iterations for FI-1	1125	1567	1608
Number of time steps for FI-0	522	519	520
Number of time steps for FI-1	522	519	520

Table 6
CPU times, number of Newton iterations, and number of time steps. Three-dimensional tetrahedral grids—case 2.

Result	1024 vertices	4056 vertices	16,810 vertices
IMPEC CPU time (s)	57.4	769.6	6395.2
FI-0 CPU time (s)	115.7	532.5	2915.7
FI-1 CPU time (s)	114.7	504.3	3025.1
Number of Newton iterations for FI-0	658	651	798
Number of Newton iterations for FI-1	684	709	838
Number of time steps for FI-0	272	207	231
Number of time steps for FI-1	272	208	231

A comparison of the production rates between the IMPEC and FI formulations is presented in Fig. 8 for the finest (hexahedral) grid. Since the results for the other elements are exactly the same, they are not shown. From Fig. 8, one can see there is a good agreement between the production rates obtained with the two FI approaches and the original IMPEC formulation of the UTCOMP simulator. We also present the saturation field at 700 days for the hexahedral grid in Fig. 9. Once again, from this figure, we can observe good agreement between the gas saturation fronts.

The CPU times, number of Newton iterations, and number of time steps for each formulation for the hexahedral, tetrahedral, prismatic, and pyramidal grids are presented in Tables 5–8, respectively. Again from these tables, one can see that the performance of the FI approaches improves as the grids are refined. The performances of the FI-0 and FI-1 approaches are very similar to each other. Once again, from Tables 5–8, one can see that the FI-1 approach required more Newton's iterations than the FI-0 approach, whereas both formulations used the same number of time steps, as expected.

Case study 3 refers to a gas flooding in a 2D irregular reservoir characterized by the following hydrocarbon components: C_1, C_3, C_6, C_{10}, C_{15}, and C_{20}. The reservoir initially contains oil, gas, and immobile water. The reservoir data used for this case

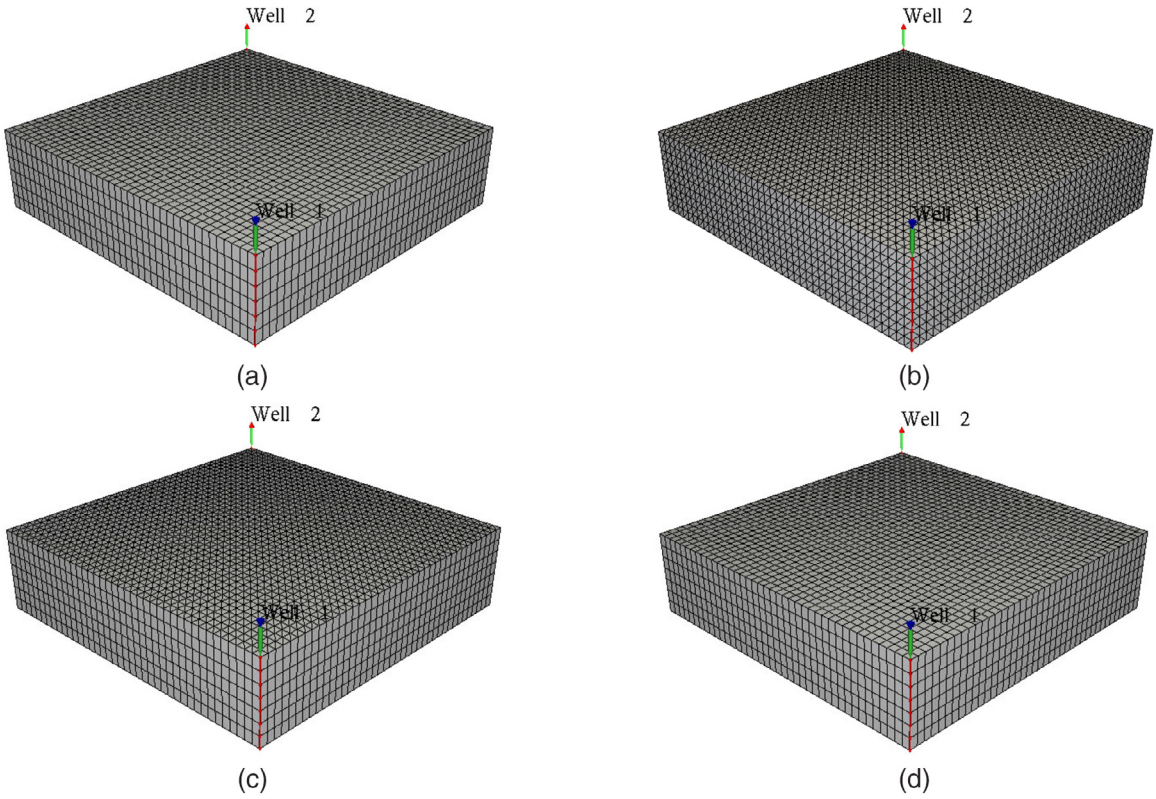

Fig. 7. Finest grids—case 2: (a) hexahedral, 11,767 vertices; (b) tetrahedral, 16,810 vertices; (c) prismatic, 13,448 vertices; (d) pyramidal, 24,648 vertices.

Table 7
CPU times, number of Newton iterations, and number of time steps. Three-dimensional prismatic grids—case 2.

Result	1024 vertices	4056 vertices	13,448 vertices
IMPEC CPU time (s)	32.4	437.5	3762.6
FI-0 CPU time (s)	65.1	359.7	2071.3
FI-1 CPU time (s)	65.7	391.4	2395.0
Number of Newton iterations for FI-0	544	584	684
Number of Newton iterations for FI-1	565	609	710
Number of time steps for FI-0	191	188	191
Number of time steps for FI-1	191	188	191

are shown in Table 9. The parameters of the equation of state for this case are shown in Tables A2 and A4, and the relative permeability parameters are presented in Table A6.

The grid used for this case is shown in Fig. 10. Two injector and six producer wells are considered for this case. All injectors are operated under constant gas injection and the producers are operated under constant bottom hole pressure. To reduce the grid orientation effect, a radial mesh is used around all the wells.

Fig. 11 presents a comparison of the production rates obtained with the two FI approaches and the IMPEC formulation. From this figures, one can observe good agreement of the production rates obtained with the three formulations.

The gas saturation fields at 6000 days of simulation for the IMPEC formulation, FI-0, and FI-1 are presented in Fig. 12. From this figure, one can observe a good agreement between the saturation fronts obtained with the three formulations.

The CPU times for all formulations are presented in Table 10. From this table, we can verify that FI-0 was faster than FI-1. One possible reason for such behavior is the increase in the number of connections of control volumes that are located between the triangular and quadrilateral elements. Once again, FI-1 used more Newton iterations than FI-0. This time, the difference in the number of Newton iterations resulted in a greater CPU time for the FI-1 approach.

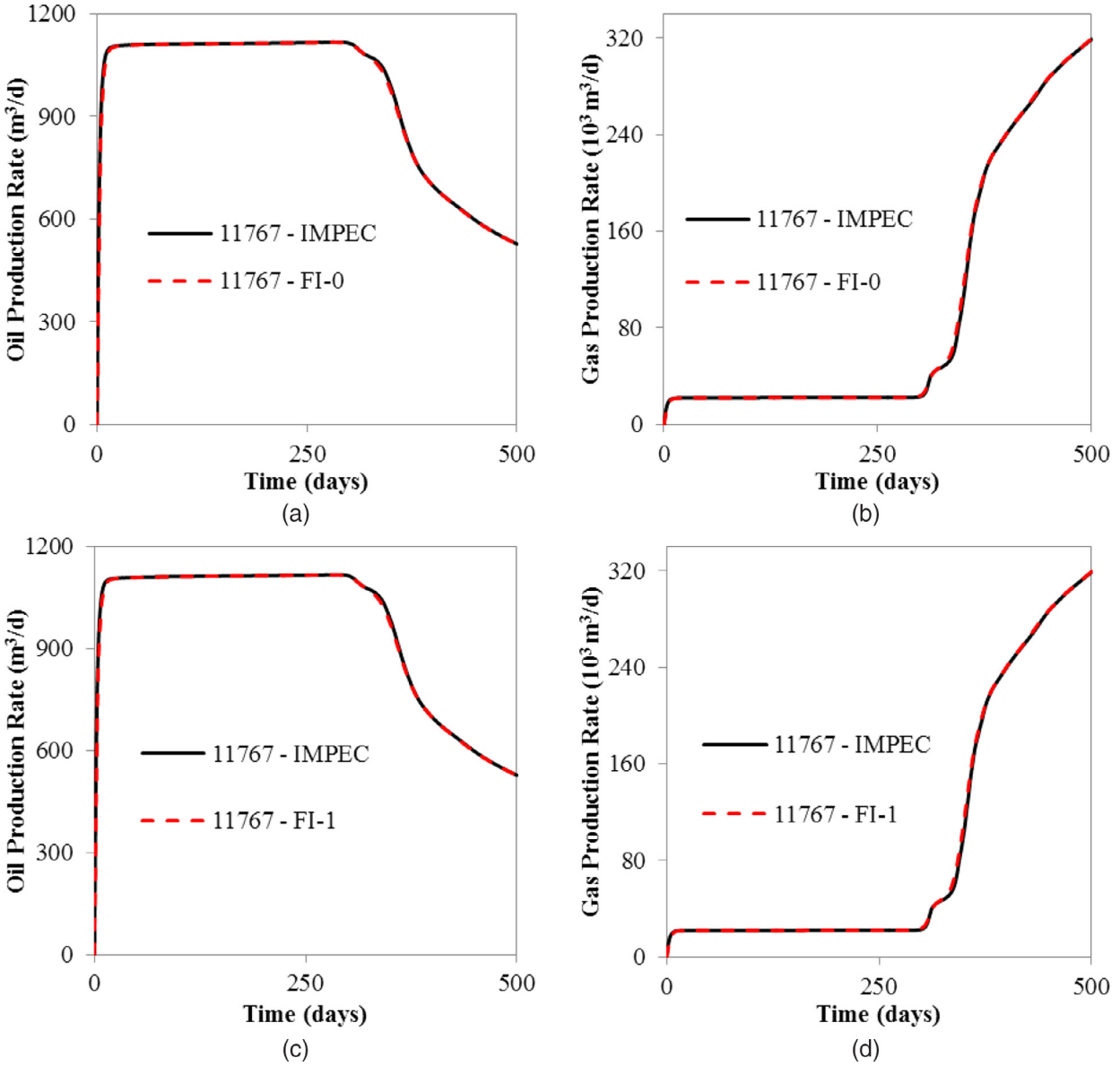

Fig. 8. Production rates—case 2 using a hexahedron grid: (a) IMPEC versus FI-0, oil; (b) IMPEC versus FI-0, gas; (c) IMPEC versus FI-1, oil; (d) IMPEC versus FI-1, gas.

Table 8
CPU times, number of Newton iterations, and number of time steps. Three-dimensional pyramidal grids—case 2.

Result	1699 vertices	7181 vertices	24,648 vertices
IMPEC CPU time (s)	98.5	1796.2	20546.0
FI-0 CPU time (s)	149.0	1169.9	5839.4
FI-1 CPU time (s)	153.9	1224.4	6137.3
Number of Newton iterations for FI-0	588	662	802
Number of Newton iterations for FI-1	600	715	891
Number of time steps for FI-0	190	191	192
Number of time steps for FI-1	190	191	192

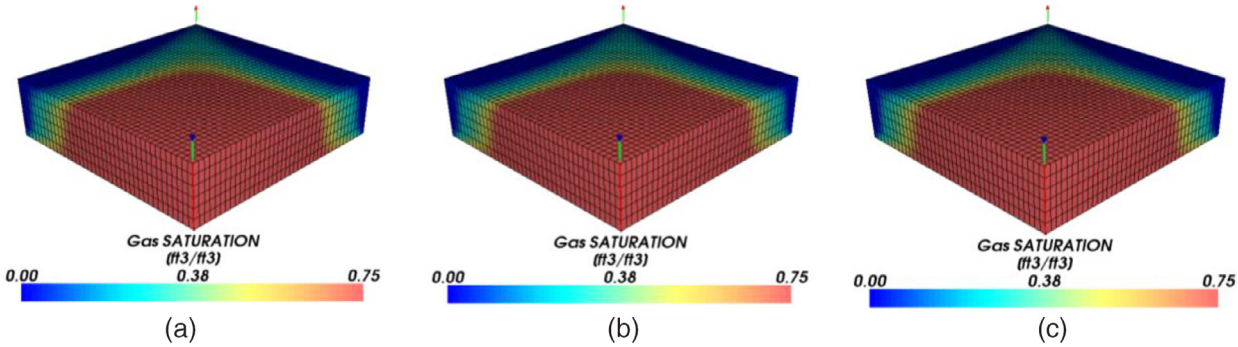

Fig. 9. Gas saturation field at 700 days—case 2 using a 3D hexahedral grid with 11767 vertices: (a) IMPEC; (b) FI-0; (c) FI-1.

Table 9
Reservoir data for case 3.

Property	Value
Superficial reservoir area and thickness	1134826.24 m^2, 30.48 m
Porosity at reference pressure	0.35
Initial water saturation	0.17
Initial pressure	10.34 MPa
Permeability in *x*, *y*, and *z* directions	1.97×10^{-14} m^2, 1.97×10^{-14} m^2, and 1.97×10^{-14} m^2
Formation temperature	344.26 K
Gas injection rate	2.83×10^5 m^3/day
Producer's bottom hole pressure	8.96 MPa
Reservoir's initial composition (C_1, C_3, C_6, C_{10}, C_{15}, and C_{20})	0.05, 0.03, 0.07, 0.20, 0.15, and 0.05
Injection fluid composition (C_1, C_3, C_6, C_{10}, C_{15}, and C_{20})	0.77, 0.20, 0.01, 0.01, 0.005, and 0.005

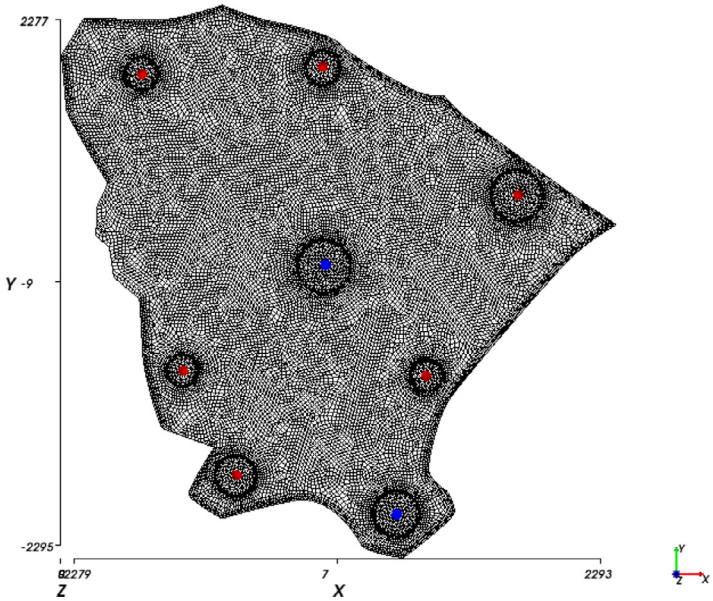

Fig. 10. Hybrid grid—case 3: 20,298 vertices; 3254 triangular and 18,195 quadrilateral elements.

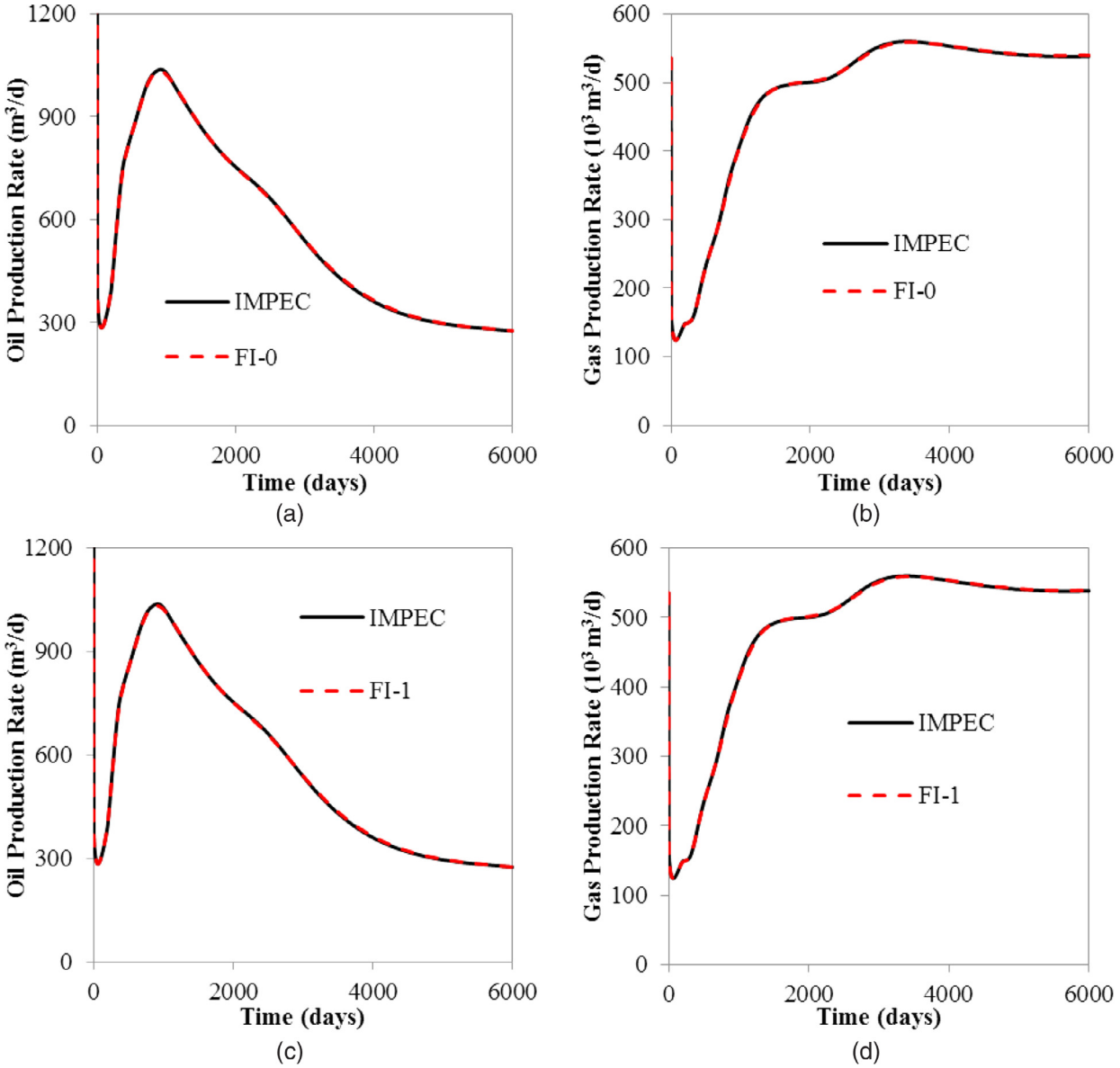

Fig. 11. Production rates—case 3: (a) IMPEC versus FI-0, oil; (b) IMPEC versus FI-0, gas; (c) IMPEC versus FI-1, oil; (d) IMPEC versus FI-1, gas.

Table 10
CPU times, number of Newton iterations, and number of time steps—case 3.

Result	Value
IMPEC CPU time (s)	6450.64
FI-0 CPU time (s)	4234.84
FI-1 CPU time (s)	4566.00
Number of Newton iterations for FI-0	1702
Number of Newton iterations for FI-1	1773
Number of time steps for FI-0	728
Number of time steps for FI-1	728

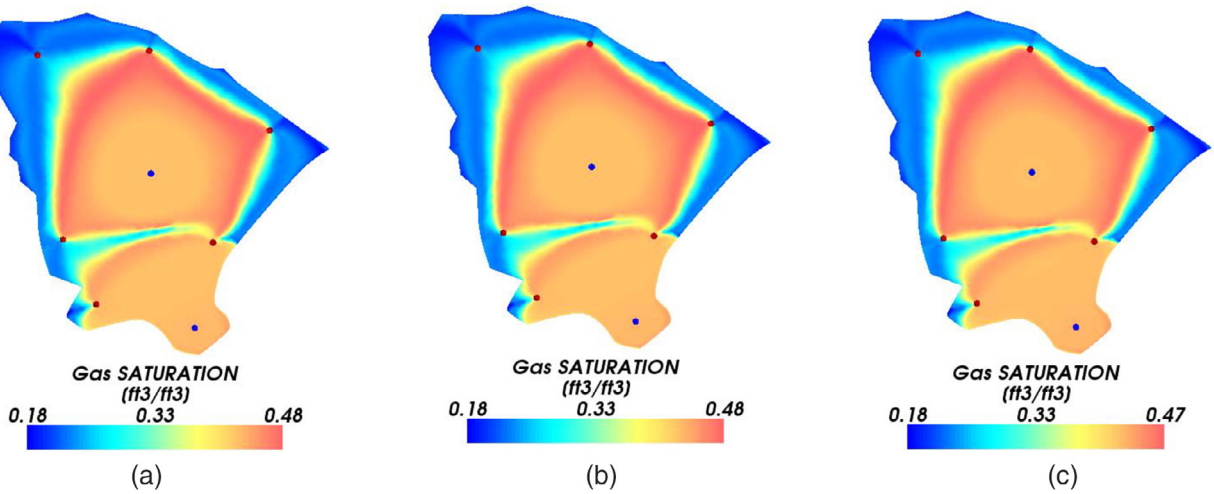

Fig. 12. Gas saturation field at 6000 days of simulation—case 3: (a) IMPEC; (b) FI-0; (c) FI-1.

5. Conclusions

In this work, two FI formulations were implemented in the UTCOMP simulator in conjunction with unstructured grids with use of the EbFVM. The new formulations were validated and compared with the IMPEC formulation originally implemented in the UTCOMP simulator.

The FI formulations have better performance when refined grids are used. However, it could not be determined which FI formulation is faster, since for some cases FI-0 was faster and for others FI-1 was faster, although we confirmed that FI-1 always required a slightly higher total number of Newton iterations. However, FI-1 has a better configuration for the UTCOMP simulator, since it shares the same set of equations as the original IMPEC formulation, which makes it easier to combine the IMPEC and FI approaches.

Acknowledgments

Bruno Ramon Batista Fernandes thanks CAPES for partial financing of this work. Also, we thank ESSS for providing Kraken® for preprocessing and postprocessing of the results. We also thank Chowdhury K. Mamun for his comments on the manuscript. Francisco Marcondes acknowledges CNPq (the National Council for Scientific and Technological Development of Brazil) for financial support through grant no. 305415/2012-3.

Tables A1–A6

Table A1
Molar mass, acentric factor, and critical properties—cases 1 and 2.

Component	P_c (MPa)	T_c (K)	V_c (m^3/mol)	Molar Mass (g/mol)	Acentric factor
CO_2	7.38	304.21	9.39×10^{-5}	44.01	0.225
C_1	4.60	190.60	9.99×10^{-5}	16.04	0.0225
C_{10}	1.74	734.68	8.17×10^{-4}	222.00	0.6837

Table A2
Molar mass, acentric factor, and critical properties—case 3.

Component	P_c (MPa)	T_c (K)	V_c (m^3/mol)	Molar Mass (g/mol)	Acentric factor
C_1	4.60	190.60	9.99×10^{-5}	16.04	0.013
C_3	4.25	369.83	2.00×10^{-4}	44.1	0.0152
C_6	3.01	507.44	3.70×10^{-4}	86.2	0.301
C_{10}	2.10	617.67	6.29×10^{-4}	142.3	0.488
C_{15}	1.38	705.56	1.04×10^{-3}	206.0	0.650
C_{20}	1.12	766.67	1.34×10^{-3}	282.0	0.850

Table A3
Binary iteration coefficients—cases 1 and 2.

Component	CO_2	C_1	C_{10}
CO_2		0.12	0.12
C_1	0.12		0
C_{10}	0.12	0	

Table A4
Binary iteration coefficients—case 3.

Component	C_1	C_3	C_6	C_{10}	C_{15}	C_{20}
C_1		0	0	0	0.05	0.05
C_3	0		0	0	0.005	0.005
C_6	0	0		0	0	0
C_{10}	0	0	0		0	0
C_{15}	0.05	0.005	0	0		0
C_{20}	0.05	0.005	0	0	0	

Table A5
Relative permeability parameters—cases 1 and 2.

Property	Value
Residual water saturation	0.3
Residual oil saturation to waterflood	0.1
Residual oil Saturation to gasflood	0.1
Residual gas saturation	0
Water relative permeability end point	0.4
Oil relative permeability end point	0.9
Gas relative permeability end point	0.9
Water exponent	3
Water exponent to waterflood	2
Oil exponent to gasflood	2
Gas exponent	2

Table A6
Relative permeability parameters—case 3.

Property	Value
Residual water saturation	0.25
Residual oil saturation to waterflood	0
Residual oil saturation to gasflood	0
Residual gas saturation	0
Water relative permeability end point	1
Oil relative permeability end point	1
Gas relative permeability end point	1
Water exponent	1
Water exponent to waterflood	1
Oil exponent to gasflood	1
Gas exponent	1

References

[1] L.T. Fussel, D.D. Fussel, An iterative technique for compositional reservoir models, SPE J. 19 (1979) 211–220.
[2] K.H. Coats, An equation of state compositional model, SPE J. 20 (1980) 363–376.
[3] L.X. Nghiem, D.K. Fong, K. Aziz, Compositional modelling with an equation of state, SPE J. 21 (1981) 687–698.
[4] L.C. Young, D.K. Stephenson, A generalized compositional approach for reservoir simulation, SPE J. 23 (1983) 727–742.
[5] M.C.H. Chien, S.T. Lee, W.H. Chen, A new fully implicit compositional simulator, in: Proceedings of the 8th SPE Symposium on Reservoir Simulation, Dallas, US, 1985.
[6] G. Ács, S. Doleschall, E. Farkas, General purpose compositional model, SPE J. 25 (1985) 543–553.
[7] H. Kazemi, C.R. Vestal, G.D. Shank, An efficient multicomponent numerical simulator, SPE J. 18 (1978) 355–368.
[8] J.W. Watts, Compositional formulation based on pressure and saturation equations, SPE Reserv. Eng. 1 (1986) 243–252.
[9] A.G. Spillette, J.G. Hillestad, H.L. Stone, A high-stability sequential solution approach to reservoir simulation, in: Proceedings of the Fall Meeting of the Society of Petroleum Engineers of AIME, Las Vegas, US, 1973.
[10] P. Quandalle, D. Savary, An implicit in pressure and saturations approach to fully compositional simulation, in: Proceedings of the 10th SPE Symposium on Reservoir Simulation, Houston, US, 1989.
[11] D.A. Collins, L.X. Nghiem, Y.-K. Li, J.E. Grabenstetter, An efficient approach to adaptive-implicit compositional simulation with an equation of state, SPE Reserv. Eng. 7 (1992) 259–264.
[12] C.M. Branco, F. Rodríguez, A semi-implicit formulation for compositional reservoir simulation, SPE Adv. Technol. Ser. 4 (1996) 171–177.

[13] P. Wang, M. Wheeler, M. Parashar, K. Sepehrnoori, A new generation eos compositional reservoir simulator: part I – formulation and discretization, in: Proceedings of the SPE Reservoir Simulation Symposium, Dallas, US, 1997.
[14] J. Haukas, I. Aavatsmark, M. Espedal, A black-oil and compositional IMPSAT Simulator with improved compositional convergence, in: Proceedings of the 9th European Conference on the Mathematics of Oil Recovery, Cannes, France, 2004.
[15] J. Haukas, I. Aavatsmark, M. Espedal, E. Reiso, A volume balance consistent compositional IMPSAT Formulation with relaxed stability constraints, Comput. Geosci (2005).
[16] L.O.S. Santos, Development of a Multi-Formulation Compositional Simulator, Department of Petroleum and Geosystems Engineering, The University of Texas at Austin, 2013 (Ph.D. dissertation).
[17] L.O.S. Santos, A. Varavei, K. Sepehrnoori, A comparison of various formulations for the compositional simulation, in: Proceedings of the SPE Reservoir Simulation Symposium, Woodlands, US, 2013.
[18] B.R.B. Fernandes, F. Marcondes, A. Varavei, K. Sepehrnoori, Comparison of an IMPEC and a semi-implicit formulation for compositional reservoir simulation, Braz. J. Chem. Eng (2014) Accepted for publication.
[19] B.R. Baliga, S.V. Patankar, A new finite-element formulation for convection-diffusion problems, Numer. Heat Transf. 3 (1980) 393–409.
[20] C.R. Maliska, Computational Heat Transfer and Fluid Mechanics, 2nd ed., LTC, Rio de Janeiro, 2004.
[21] Z.E. Heinemann, C.W. Brand, Gridding techniques in reservoir simulation, in: Proceedings of the 1st International Forum on Reservoir Simulation, Apbach, Austria, 1988.
[22] Z.E. Heinemann, C.W. Brand, M. Munka, Y.M. Chen, Modelling reservoir geometry with irregular grids, SPE Reserv. Eng. 6 (1991) 225–232.
[23] B.J. Rozon, A generalized finite volume method for reservoir simulation, in: Proceedings of the Reservoir Simulation Symposium, Houston, US, 1989.
[24] L.S.-K. Fung, A.D. Hiebert, L.X. Nghiem, Reservoir simulation with a control-volume finite-element method, SPE Reserv. Eng. 7 (1992) 349–357.
[25] J. Cordazzo, Petroleum Reservoir Simulation Using the Ebfvm Method and Algebraic Multigrid, Department of Mechanical Engineering, Federal University of Santa Catarina, 2006 Ph.D. dissertation.
[26] F. Marcondes, K. Sepehrnoori, An element-based finite volume-method approach for heterogeneous and anisotropic compositional reservoir simulation, J. Pet. Sci. Eng 73 (2010) 99–106.
[27] F. Marcondes, L.O.S. Santos, A. Varavei, K. Sepehrnoori, A 3D hybrid element-based finite volume method for heterogeneous and anisotropic compositional reservoir simulation, J. Pet. Sci. Eng 108 (2013) 342–351.
[28] L.O.S. Santos, F. Marcondes, K. Sepehrnoori, A 3D compositional miscible gas flooding simulator with dispersion using element-based finite-volume method, J. Pet. Sci. Eng 112 (2013) 61–68.
[29] B.R.B. Fernandes, F. Marcondes, K. Sepehrnoori, Investigation of several interpolation functions for unstructured meshes in conjunction with compositional simulation, Numer. Heat Transf. Part A: Appl 64 (2013) 974–993.
[30] B.R.B. Fernandes, A.D.R. Gonçalves, E.P. Drumond Filho, I.C.M. Lima, F. Marcondes, K. Sepehrnoori, A3D total variation diminishing scheme for compositional reservoir simulation using the element-based finite volume method, Numer. Heat Transf. Part A: Appl 46 (2015) 839–856.
[31] M.S. Darwish, F. Moukalled, TVD schemes for unstructured grids, Int. J. Heat Mass Transf. 46 (2003) 599–611.
[32] P.L. Roe, Some Characteristic-based schemes for the euler equations, Ann. Rev. Fluid Mech 18 (1986) 337–365.
[33] B. Koren, A Robust Upwind discretization method for advection, diffusion and source terms, in: C.B. Vreugdenhil, B. Koren (Eds.), Numerical Methods for Advection-Diffusion Problems, Notes on Numerical Fluid Mechanics, vol. 45, Vieweg, Braunschweig, 1993, pp. 117–138.
[34] Y.-B. Chang, Development and Application of an Equation of State Compositional Simulator, (Ph.D. dissertation), Department of Petroleum and Geosystems Engineering, The University of Texas at Austin, 1990.
[35] B.R.B. Fernandes, Compositional Petroleum Reservoir Simulation Using the Element Based Finite Volume Method, (B.Sc. thesis), Department of Chemical Engineering, Federal University of Ceara, 2011.
[36] B.R.B. Fernandes, I.C.M. Lima, A.L.S. Araújo, F. Marcondes, K. Sepehrnoori, 2D compositional reservoir simulation using unstructured grids in heterogeneous reservoirs, in: Proceedings of the 10th Congress on Computational Mechanics, São Paulo, Brazil, 2012.
[37] A.L.S. Araújo, B.R.B. Fernandes, R.M. Araujo, E.P. Drumond Filho, I.C.M. Lima, F. Marcondes, K. Sepehrnoori, 3D compositional reservoir simulation using unstructured grids in homogeneous reservoirs, in: Proceedings of the COBEM 2013, RibeirãoPreto, Brazil, 2013.
[38] M.G. Doroh, Development and Application of a Parallel Compositional Reservoir Simulator, Department of Petroleum and Geosystems Engineering, The University of Texas at Austin, 2012 Master thesis.
[39] P. Wang, S. Balay, K. Sepehrnoori, J. Wheeler, J. Abate, B. Smithe, G.A. Pope, A fully implicit parallel eos compositional simulator for large scale reservoir simulation, Paper SPE 51885, Fifteenth Symposium on Reservoir Simulation (February 1999) Houston, TX.
[40] D.-Y. Peng, D.B. Robinson, A new two-constant equation of state, Ind. Eng. Chem. Fundam 15 (1976) 59–64.
[41] J.L. Michelsen, The isothermal flash problem. Part I. Stability, Fluid Phase Equilibria 9 (1982) 1–19.
[42] J.A. Trangenstein, Customized minimization techniques for phase equilibrium computations in reservoir simulation, Chem. Eng. Sci 42 (1988) 2847–2863.
[43] D.R. Perschke, Equation of State Phase Behavior Modelling for Compositional Simulator, Department of Petroleum and Geosystems Engineering, The University of Texas at Austin, 1988 Ph.D. dissertation.
[44] A.R. Mehra, R.A. Heidemann, K. Aziz, An accelerated successive substitution algorithm, Can. J. Chem. Eng 61 (1983) 590–596.
[45] B.R.B. Fernandes, Implicit and Semi-Implicit Techniques for the Compositional Petroleum Reservoir Simulation Based on Volume Balance, (Master thesis), Department of Chemical Engineering, Federal University of Ceara, 2014.
[46] S. Balay, M.F. Adams, J. Brown, P. Brune, K. Buschelman, V. Eijkhout, W.D. Gropp, D. Kaushik, M.G. Knepley, L.C. Mcinnes, K. Rupp, B.F. Smith, and H. Zhang, PETSc User's Manual, http://www.mcs.anl.gov/petsc, Argone National Laboratory, 2014.
[47] Y. Saad, M.H. Schultz, GMRES: A generalized minimal residual algorithm for solving nonsymmetrical linear systems, SIAM J. Sci. Stat. Comput. 7 (1986) 856–869.
[48] X. Li, A Collection of Case Studies for Verification of Reservoir Simulators, (Master thesis), Department of Petroleum and Geosystems Engineering, The University of Texas at Austin, 2012.
[49] H.L. Stone, Estimation of three-phase relative permeability and residual oil data, J. Can. Pet. Technol 10 (1973) 53–61.